J. Ocean Eng. Mar. Energy (2015) 1:3–18
DOI 10.1007/s40722-014-0001-3

RESEARCH ARTICLE

Radiation and oblique diffraction by submerged prolate spheroids in water of finite depth

Ioannis K. Chatjigeorgiou · Touvia Miloh

Received: 21 May 2014 / Accepted: 4 July 2014 / Published online: 25 September 2014

Abstract In the present study we present a general methodology for estimating the hydrodynamic (added-mass and damping) coefficients of a fully submerged (below a free-surface) elongated axisymmetric ocean-going body (approximated by a prolate spheroid) in water of finite depth (rigid even sea bottom). Using the same approach, we also provide a solution for the corresponding linearized diffraction problem and analytically determine the exciting hydrodynamic forces and moments exerted on the body due to obliquely incident monochromatic surface waves. A comprehensive series of numerical simulations is presented for the relevant hydrodynamic parameters depending on the wave encounter frequency and angle of incidence, including body submergence and slenderness-ratio as well as the water depth. Numerical validations are also provided as limiting cases for spherical shapes in finite water and for spheroidal geometries in water of infinite depth.

Keywords Prolate spheroids · Spheroidal harmonics · Multipole expansions · Green's function · Oblique diffraction · Hydrodynamic coefficients

1 Introduction

The hydrodynamics of axisymmetric bodies of revolution have been studied for decades. In that respect, the most efficient and difficult to develop methods are those based on linearized analytical approaches. In most of the cases, the difficulties are associated with the laborious mathematical elaboration that is required. As a result, the majority of the existing studies use several simplifications, out of which the most popular are the geometry and the water depth. It is evident that the bulk of the publications on the hydrodynamics and in particular on the radiation and the diffraction problems, of axisymmetric bodies concern perfectly symmetric spherical objects. Those are indeed the most commonly used geometries and it is a fact that they have been thoroughly studied covering all possible hydrodynamical aspects for both deep (infinite) and finite (constant) water depths.

Havelock (1955) was probably the first to provide an analytic solution to the heave radiation problem of a half-immersed sphere in deep water. Accordingly, Hulme (1982) improved and extended the work of Havelock (1955) to the case of sway. Gray (1979) considered only the scattering problem for a submerged sphere in a sea of infinite water depth by formulating the problem as an integral equation. Srokosz (1979) used a different line of approach for a submerged sphere to study simultaneously the heave and sway radiation problems in deep water by adopting the method of multipoles, which was first suggested by Ursell (1950) for submerged circular cylinders oscillating below a free-surface. Finally Wang (1986) employed the method of Havelock (1955) to solve both the radiation and the diffraction problems for a submerged sphere. However, the assumption of an infinite water depth was again considered.

As far as the hydrodynamics of spheres is concerned, Thorne (1953) pioneering contribution on multipole potentials for both deep and finite water depths, made the subsequent efforts easier. Among the studies which employed Thorne (1953) multipole expansions for submerged spheres were those due to Linton (1991), Wu et al. (1994), Rahman

I. K. Chatjigeorgiou (✉)
School of Naval Architecture and Marine Engineering,
National Technical University of Athens, Athens, Greece
e-mail: chatzi@naval.ntua.gr

T. Miloh
Faculty of Engineering, Tel-Aviv University, Tel Aviv, Israel

(2001) and Das and Mandal (2008) (in chronological order). All these studies assumed the general case of finite (constant) water depth over a rigid flat bottom. In particular, Linton (1991) solved both the diffraction and radiation problems, Wu et al. (1994) evaluated the hydrodynamic loads including the drift forces, Rahman (2001) considered only the exciting forces, whilst Das and Mandal (2008) tackled only the radiation problem, but assuming that the sphere was submerged below an ice cover floating on the free surface. Thorne (1953) multipole potentials were also employed for spheroids, both oblate (Chatjigeorgiou 2012) and prolate (Chatjigeorgiou 2013). In particular, Chatjigeorgiou (2012, 2013), succeeded to transform the multipole potentials associated with the infinite water depth case, originally expressed in spherical and polar coordinates, to prolate and oblate spheroidal coordinates in order to apply the Neumann body boundary condition. Both studies however considered only axisymmetric spheroids (semi-major axis perpendicular to the free surface) and only the diffraction problem.

Although the corresponding linearized hydrodynamic problems employing spherical shapes have been all well treated in the literature, both for deep and finite water depths, related studies on more practical shapes of ocean going vehicles that can be simulated mathematically as prolate spheroids are not very common. In fact, to the authors' best knowledge, only cases of deep water have been considered so far for the diffraction and radiation problems of submerged spheroids. Throughout this paper the term "spheroid" will refer to prolate spheroids of arbitrary eccentricity and in particular to the non-axisymmetric configuration, namely when the horizontal semi-major axis is parallel to the free surface, which is apparently the most relevant case. The diffraction problem for submerged spheroids in deep water was considered by Wu and Eatock Taylor (1987) and Chatjigeorgiou and Miloh (2013), whereas Chatjigeorgiou and Miloh (2014a) included the effect of forward speed as well. In the former study (Wu and Eatock Taylor 1987) the authors considered only head seas and provided data for a limited range of frequencies. Accordingly, Wu and Eatock Taylor (1989) extended their deep-water formulation to study both the oblique diffraction and the radiation problems. Wu and Eatock Taylor (1987, 1989) based their formulation on the numerical solution of a Fredholm integral equation of the second kind, involving a source/sink distribution over the surface of the spheroid that was originally proposed by Farell (1973) for tackling the hydrodynamic wave resistance problem. For solving the wave diffraction problem by prolate spheroids in infinite water depth, Chatjigeorgiou and Miloh (2013, 2014a) followed a different line of approach. In particular they used the method of interior image singularities developed by Miloh (1974). In fact, obtaining analytic solutions for the wave diffraction (Wu and Eatock Taylor 1987; Chatjigeorgiou and Miloh 2013, 2014a), radiation (Wu and Eatock Taylor 1989) and the wave resistance (Farell 1973) problems by non-axisymmetric submerged spheroids became feasible by virtue of the expansion of the monochromatic wave potential in spheroidal harmonics, as originally proposed by Havelock (1954).

The current study aims at covering the lack of analytic formulations for the classical hydrodynamic linearized free-surface *radiation* and *oblique* wave diffraction problems of submerged spheroids in *finite* water depths. To this end, we follow the methodology recently presented in Chatjigeorgiou and Miloh (2014b) and tackle both the hydrodynamic diffraction and the radiation problems in one single effort. The solution is achieved by using the ultimate image singularity system of external spheroidal harmonics distributed along the major axis of the spheroid between its two foci. For the finite water depth case however, the governing Green's function is different and the complications are accordingly reflected in the effort required for developing an efficient solution algorithm.

The organization of the paper is as follows: In Sect. 2 we present the general linearized working equations for both radiation and diffraction problem and in Sect. 3 we give a general expression for the Green's function using spheroidal harmonics for the combined case. The solution of the radiation problem, including explicit expressions for both added-mass and damping coefficients in terms of exciting frequencies, submergence and water depth, is given in Sect. 4. Also presented in Sect. 5 are general expressions for the hydrodynamic forces and moments exerted on the body due to a monochromatic wave-train at oblique angle of incidence with respect to the body's major axis. An extensive set of numerical simulations is then given and plotted in Sect. 6, both for the various hydrodynamic coefficients and exciting forces and moments acting on the spheroid depending on problem parameters such as: encounter frequency, depth of submergence, water depth, angle of wave incidence etc. Validations against solutions for spherical geometries or for spheroids operating in water of infinite depth are also given, including simulations for the extreme case of a bottom seated elongated spheroidal-like shape. We conclude in Sect. 7 with a short discussion and summary.

2 Formulation of the hydrodynamic problem

The prolate spheroid is assumed to be immersed under a free upper surface and above a flat bottom of finite depth h. A left-handed Cartesian (x, y, z) coordinate system is considered, fixed on the free surface with the vertical z axis pointing in the gravity direction. The immersion of the center of the spheroid relatively to the (x, y, z) system is f. Thus, the body fixed Cartesian system is (x, y, z^*)(z^* also pointing downwards) with $z = z^* + f$. The semi-major axis of

the body is parallel to the free surface defining the so-called "non-axisymmetric" case. The transformation between prolate spheroidal and Cartesian coordinates for the body fixed system is

$$x = c\mu\zeta \tag{1}$$
$$y = c\sqrt{\zeta^2-1}\sqrt{1-\mu^2}\sin\psi \tag{2}$$
$$z^* = c\sqrt{\zeta^2-1}\sqrt{1-\mu^2}\cos\psi \tag{3}$$

where c is the half distance between the foci with $c = \sqrt{a^2-b^2}$ and a, b are the semi-major and the semi-minor axis respectively. We have chosen to employ (Nicholson 1924) notation (ζ, μ, ψ), $\zeta = \cosh u$, $\mu = \cos\vartheta$ for the spheroidal coordinate system instead of using the traditional spheroidal coordinates (u, ϑ, ψ), $0 \le u < \infty$, $0 \le \vartheta \le \pi$ and $0 \le \psi < 2\pi$. Throughout this paper we will employ dimensionless representations where lengths are normalized with respect to the half distance between the foci (equivalent to letting $c = 1$).

For time harmonic motions of the body the velocity potential is written as $\Phi = \mathrm{Re}(\phi e^{i\omega t})$, where ω is the circular frequency of oscillations. In the realm of the linear theory, the time-independent potential must satisfy the Laplace equation

$$\nabla^2\phi = 0 \tag{4}$$

in the fluid domain. The common linearized free surface boundary condition on $z = 0$ is given by

$$K\phi + \frac{\partial\phi}{\partial z} = 0, \tag{5}$$

where $K = \omega^2/g$ (g is the gravitational acceleration) and the boundary condition on the flat bottom at $z = h$ is

$$\frac{\partial\phi}{\partial z} = 0, \tag{6}$$

assuming that the bottom is horizontal. It is understood that the velocity potential must also satisfy a proper radiation condition for outgoing waves at infinity. In Eqs. (4)–(6) ϕ denotes the total velocity potential which is given by

$$\phi = \phi_\mathrm{I} + \phi_\mathrm{D} + i\omega\sum_{j=1}^{6}\xi_j\phi_j \tag{7}$$

where ϕ_I is the incident wave component, ϕ_D is the diffraction component whilst ϕ_j denotes the six radiation (Kirchhoff) potentials for the six modes of motion, three translational for $j = 1, 2, 3$ (surge, sway, heave) and three rotational for $j = 4, 5, 6$ (roll, pitch, yaw) with amplitudes ξ_j. The formulation of the hydrodynamic problem is completed by introducing the appropriate impermeable body boundary condition which must be satisfied separately for the diffraction and the radiation problems. These are

$$\frac{\partial(\phi_\mathrm{D}+\phi_\mathrm{I})}{\partial n} = 0, \tag{8}$$

and

$$\frac{\partial\phi_j}{\partial n} = n_j, \quad j = 1, 2, 3, 4, 5, 6, \tag{9}$$

where $\mathbf{n} = (n_1, n_2, n_3)$ is the outward normal (directed into the fluid) on the body surface S_0 and $\mathbf{r}$ is the radius vector of a point on the surface such that $(\mathbf{r}\times\mathbf{n}) = (n_4, n_5, n_5)$.

3 The Green's function and its expansion into spheroidal harmonics

According to the employed assumptions the Green's function, expressed in Cartesian coordinates, that satisfies the Laplace equation and the bottom boundary condition can be written as Wehausen and Laitone (1960)

$$\begin{aligned} G(x,y,z) = {} & \frac{1}{r} + \frac{1}{r'} \\ & + \frac{1}{\pi}\mathrm{PV}\int_0^\infty\int_{-\pi}^{\pi} Q^*(k,h)\cosh k(h-z) \\ & \times e^{ik(x\cos a + y\sin a)}\,\mathrm{d}a\,\mathrm{d}k \\ & + i\int_{-\pi}^{\pi} Q_0^*(k_0,h)\cosh k_0(h-z) \\ & \times e^{ik_0(x\cos a + y\sin a)}\,\mathrm{d}a, \end{aligned} \tag{10}$$

where

$$r = \sqrt{x^2+y^2+(z-f)^2},$$
$$r' = \sqrt{x^2+y^2+(z+f-2h)^2} \tag{11}$$

and

$$Q^*(k,h) = \frac{2e^{-kh}(K+k)\cosh k(h-f)}{K\cosh kh - k\sinh kh}, \tag{12}$$

$$Q_0^*(k_0,h) = \frac{(K+k_0)e^{-k_0h}\cosh k_0(h-f)\sinh k_0h}{Kh+\sinh^2 k_0h}. \tag{13}$$

In Eq. (13) k_0 denotes the root of the well-known dispersion relation

$$K = k_0\tanh k_0h, \tag{14}$$

whilst PV in Eq. (10) denotes the Cauchy principal value integral.

The original Green's function is next elaborated using Miloh (1974) integral expression for the spheroidal ultimate

image singularity system. This is

$$P_n^m(\mu)Q_n^m(\zeta)\mathrm{e}^{im\psi} = \frac{1}{2}\left(\frac{\partial}{\partial z} + i\frac{\partial}{\partial y}\right)^m \times \int_{-1}^{1} \frac{(1-\lambda^2)^{m/2}P_n^m(\lambda)}{\sqrt{(x-\lambda)^2+y^2+z^2}}\mathrm{d}\lambda. \quad (15)$$

where P_n^m and Q_n^m denote the n-th degree and m-th order associate Legendre functions of the first and the second kind respectively. Also, we choose to reverse the orientations of the vertical axes z and z^* which will now be connected by $z = z^* - f$. By combining Eqs. (10) and (15), one gets after tedious mathematical manipulations the auxiliary multipole expansions G_n^m of the Green's function which satisfy both the linearized free-surface and rigid bottom boundary conditions given by Eqs. (5)–(6). For the details of the mathematical analysis and the various transformations which were required, we refer the reader to the recent studies of the same authors (Chatjigeorgiou and Miloh 2014a, b). In particular the auxiliary multipole expansions of the Green's function G_n^m will admit the following form;

$$G_n^m(x,y,z) = P_n^m(\mu)Q_n^m(\zeta)\mathrm{e}^{im\psi} + \sum_{s=0}^{\infty}\sum_{t=0}^{s}\left(C_{ns}^{mt}\cos t\psi + i\tilde{C}_{ns}^{mt}\sin t\psi\right) \times P_s^t(\mu)P_s^t(\zeta). \quad (16)$$

where the various coefficients are defined below as

$$C_{ns}^{mt} = R_{ns}^{mt} + D_{ns}^{mt} + i\pi E_{ns}^{mt},$$
$$\tilde{C}_{ns}^{mt} = \tilde{R}_{ns}^{mt} + \tilde{D}_{ns}^{mt} + i\pi \tilde{E}_{ns}^{mt} \quad (17)$$

$$R_{ns}^{mt} = \frac{\varepsilon_t}{4}(-1)^{n+m+t}i^{n+m+s+t}\frac{(n+m)!}{(n-m)!}\frac{(s-t)!}{(s+t)!} \times (2s+1)\int_0^{\pi/2}\frac{N_m(a)N_t(a)}{\cos a} \times \int_0^{\infty}\frac{\mathrm{e}^{-2k(h-f)}}{k}J_{n+1/2}(k\cos a) \times J_{s+1/2}(k\cos a)\mathrm{d}a\mathrm{d}k. \quad (18)$$

$$D_{ns}^{mt} = \frac{\varepsilon_t}{4}(-1)^{n}i^{n+m+s+t}\frac{(n+m)!}{(n-m)!}\frac{(s-t)!}{(s+t)!}(2s+1) \times \int_0^{\pi/2}\frac{N_m(a)N_t(a)}{\cos a} \times \mathrm{PV}\int_0^{\infty}Q^*(k,h)\frac{\mathrm{e}^{k(h-f)}+(-1)^{m+t}\mathrm{e}^{-k(h-f)}}{k} \times J_{n+1/2}(k\cos a)J_{s+1/2}(k\cos a)\mathrm{d}a\mathrm{d}k, \quad (19)$$

$$E_{ns}^{mt} = \frac{\varepsilon_t}{4}(-1)^{n}i^{n+m+s+t}\frac{(n+m)!}{(n-m)!}\frac{(s-t)!}{(s+t)!} \times (2s+1)Q_0^*(k_0,h)\frac{\mathrm{e}^{k_0(h-f)}+(-1)^{m+t}\mathrm{e}^{-k_0(h-f)}}{k_0} \times \int_0^{\pi/2}\frac{N_m(a)N_t(a)}{\cos a}J_{n+1/2} \times (k\cos a)J_{s+1/2}(k\cos a)\mathrm{d}a, \quad (20)$$

$$N_t(a) = \frac{(1+\sin a)^t + (1-\sin a)^t}{(\cos a)^t},$$
$$\tilde{N}_t(a) = \frac{(1+\sin a)^t - (1-\sin a)^t}{(\cos a)^t} \quad (21)$$

Note that J notes the Bessel function of the first-kind, $\varepsilon_0 = 1$, $\varepsilon_t = 2$ for $t = 1, 2, \ldots$, whilst $\tilde{R}_{ns}^{mt}$, $\tilde{D}_{ns}^{mt}$ and $\tilde{E}_{ns}^{mt}$ are obtained respectively by Eqs. (18), (19) and (20) by simply replacing $N_m(a)N_t(a)$ by $\tilde{N}_m(a)\tilde{N}_t(a)$. Also, all expansion coefficients R_{ns}^{mt}, D_{ns}^{mt}, E_{ns}^{mt}, $\tilde{R}_{ns}^{mt}$, $\tilde{D}_{ns}^{mt}$ and $\tilde{E}_{ns}^{mt}$ are nonzero only if $n+m+s+t$ is even and they vanish accordingly if $n+m+s+t$ is odd.

The most difficult part as regards the numerical implementation of the developed methodology is the accurate computation of the PV integral. To this end, one could proceed further analytically, to reduce the numerical effort, by expanding the Bessel functions into ascending series (Abramowitz and Stegun 1970; Watson 1944). However, the employment of the ascending series in the present problem has significant limitations since for small water depths and small body submergence the results are not convergent. Hence, all integrals have been computed here numerically. For the PV integrals we relied on the efficiency of the Sinc quadrature algorithm developed by Bialecki and Keast (1999), whereas for the definite integrals we employed the Gauss–Legendre quadrature formula (Press et al. 1986).

4 The radiation problem: radiation potentials and hydrodynamic coefficients

The body boundary conditions [Eq. (9)], associated with the radiation potentials for both the translational and the rotational modes of motion, can be expresses as

$$\left.\frac{\partial\phi_1}{\partial u}\right|_{u=u_0} = b\mu = bP_1^0(\mu) \quad (22)$$

$$\left.\frac{\partial\phi_2}{\partial u}\right|_{u=u_0} = a\sqrt{1-\mu^2}\sin\psi = -aP_1^1(\mu)\sin\psi \quad (23)$$

$$\left.\frac{\partial\phi_3}{\partial u}\right|_{u=u_0} = a\sqrt{1-\mu^2}\cos\psi = -aP_1^1(\mu)\cos\psi \quad (24)$$

$$\left.\frac{\partial\phi_4}{\partial u}\right|_{u=u_0} = 0 \quad (25)$$

$$\left.\frac{\partial\phi_5}{\partial u}\right|_{u=u_0} = (b^2-a^2)\sqrt{1-\mu^2}\mu\cos\psi$$
$$= \frac{a^2-b^2}{3}P_2^1(\mu)\cos\psi \quad (26)$$
$$\left.\frac{\partial\phi_6}{\partial u}\right|_{u=u_0} = (a^2-b^2)\sqrt{1-\mu^2}\mu\sin\psi$$
$$= -\frac{a^2-b^2}{3}P_2^1(\mu)\sin\psi \quad (27)$$

where $u_0 = \tanh^{-1}(b/a)$. Using the axillary multipole expansions of the Green's function [Eq. (16)], all six radiation potentials can be written as

$$\phi_j = \sum_{n=0}^{\infty}\sum_{m=0}^{n} F_n^m \left\{ P_n^m(\mu)Q_n^m(\zeta)\mathrm{e}^{im\psi} + \sum_{s=0}^{\infty}\sum_{t=0}^{s}(C_{ns}^{mt}\cos t\psi + i\tilde{C}_{ns}^{mt}\sin t\psi) \times P_s^t(\mu)P_s^t(\zeta)\right\} \quad (28)$$

Introducing Eq. (28) into the body boundary conditions given by Eqs. (22)–(24) and (26)–(27) (roll motion is ignored due to axial symmetry) and making use of the orthogonality relations of the trigonometric and the Associate Legendre functions of the first kind (Abramowitz and Stegun 1970), we obtain five systems of linear equations that provide the unknown expansion coefficients for surge, sway, heave, pitch and yaw, i.e.

$$F_l^r + \alpha_l^r \sum_{n=0}^{\infty}\sum_{m=0}^{n} F_n^m C_{nl}^{mr} = \frac{\delta_{0r}\delta_{1l}}{\dot{Q}_l^r(\zeta_0)}, \quad (29)$$
$$\tilde{F}_l^r + \alpha_l^r \sum_{n=0}^{\infty}\sum_{m=0}^{n} \tilde{F}_n^m \tilde{C}_{nl}^{mr} = i\frac{a}{b}\frac{\delta_{1r}\delta_{1l}}{\dot{Q}_l^r(\zeta_0)}, \quad (30)$$
$$F_l^r + \alpha_l^r \sum_{n=0}^{\infty}\sum_{m=0}^{n} F_n^m C_{nl}^{mr} = -\frac{a}{b}\frac{\delta_{1r}\delta_{1l}}{\dot{Q}_l^r(\zeta_0)}, \quad (31)$$
$$F_l^r + \alpha_l^r \sum_{n=0}^{\infty}\sum_{m=0}^{n} F_n^m C_{nl}^{mr} = \frac{a^2-b^2}{3b}\frac{\delta_{1r}\delta_{2l}}{\dot{Q}_l^r(\zeta_0)}, \quad (32)$$
$$\tilde{F}_l^r + \alpha_l^r \sum_{n=0}^{\infty}\sum_{m=0}^{n} \tilde{F}_n^m \tilde{C}_{nl}^{mr} = i\frac{a^2-b^2}{3b}\frac{\delta_{1r}\delta_{2l}}{\dot{Q}_l^r(\zeta_0)}, \quad (33)$$

where $\alpha_l^r = \frac{\dot{P}_l^r(\zeta_0)}{\dot{Q}_l^r(\zeta_0)}$ and the upper dot represents differentiation with respect to the argument. Equations (29)–(33) assume by default that $c = 1$ and they are valid sequentially for the surge, sway, heave, pitch and yaw modes of motion.

Having calculated all the radiation potentials, the corresponding hydrodynamic masses and damping coefficients can be next determined from the following surface integral

$$\mu_{ij} - \frac{i}{\omega}\lambda_{ij} = -\rho\int_{S_0}\phi_i n_j \mathrm{d}S \quad (34)$$

where μ_{ij}, λ_{ij} denote respectively the added masses and the damping coefficients (ρ is the water density), whilst the integration is performed on the wetted surface of the spheroid S_0.

The outward normal for the translational and the rotational modes are given by

$$(n_1, n_2, n_3) = \left[\frac{(\zeta_0^2-1)^{1/2}\mu}{(\zeta_0^2-\mu^2)^{1/2}}, \frac{\zeta_0(1-\mu^2)^{1/2}\sin\psi}{(\zeta_0^2-\mu^2)^{1/2}}, \frac{\zeta_0(1-\mu^2)^{1/2}\cos\psi}{(\zeta_0^2-\mu^2)^{1/2}}\right] \quad (35)$$

and for the rotational modes by

$$(n_5, n_6) = (b^2-a^2) \times \left[\frac{\mu(1-\mu^2)^{1/2}\cos\psi}{c(\zeta_0^2-\mu^2)^{1/2}}, -\frac{\mu(1-\mu^2)^{1/2}\sin\psi}{c(\zeta_0^2-\mu^2)^{1/2}}\right] \quad (36)$$

The differential area $\mathrm{d}S$ is written in spheroidal coordinates as

$$\mathrm{d}S = c^2(\zeta_0^2-1)^{1/2}(\zeta_0^2-\mu^2)^{1/2}\mathrm{d}\mu\mathrm{d}\psi. \quad (37)$$

After introducing Eq. (28) and Eqs. (35)–(37) into Eq. (34) and performing the integrations, we obtain for the diagonal terms μ_{jj}, λ_{jj} the following relations

$$\mu_{11} - \frac{i}{\omega}\lambda_{11} = -\frac{1}{a}\left[F_1^0 Q_1^0(\zeta_0) + \sum_{n=0}^{\infty}\sum_{m=0}^{n} F_n^m C_{n1}^{m0} P_1^0(\zeta_0)\right] \quad (38)$$
$$\mu_{22} - \frac{i}{\omega}\lambda_{22} = \frac{i}{b}\left[F_1^1 Q_1^1(\zeta_0) + \sum_{n=0}^{\infty}\sum_{m=0}^{n} F_n^m \tilde{C}_{n1}^{m1} P_1^1(\zeta_0)\right] \quad (39)$$
$$\mu_{33} - \frac{i}{\omega}\lambda_{33} = \frac{1}{b}\left[F_1^1 Q_1^1(\zeta_0) + \sum_{n=0}^{\infty}\sum_{m=0}^{n} F_n^m C_{n1}^{m1} P_1^1(\zeta_0)\right] \quad (40)$$
$$\mu_{55} - \frac{i}{\omega}\lambda_{55} = 3\frac{b^2-a^2}{a^3 b} \times \left[F_2^1 Q_2^1(\zeta_0) + \sum_{n=0}^{\infty}\sum_{m=0}^{n} F_n^m C_{n2}^{m1} P_2^1(\zeta_0)\right] \quad (41)$$

$$\mu_{66} - \frac{i}{\omega}\lambda_{66} = 3i\frac{a^2-b^2}{a^3 b} \times \left[F_2^1 Q_2^1(\zeta_0) + \sum_{n=0}^{\infty}\sum_{m=0}^{n} F_n^m \tilde{C}_{n2}^{m1}\, P_2^1(\zeta_0) \right] \tag{42}$$

where $\mu_{44} = \lambda_{44} = 0$ due to axial symmetry. The translational modes have been normalized by $4/3\pi\rho ab^2$ and the rotational modes by $4/15\pi\rho a^3 b^2$. Thus, the added mass coefficients are non-dimensional whilst the damping coefficients have dimension 1/s.

5 The diffraction problem and the exciting forces

The incident wave potential for a monochromatic wave train of amplitude A and circular frequency ω propagating in a fluid domain of finite depth h, at angle β with respect to the horizontal x-axis that coincides with the spheroid's semi-major axis is written as

$$\phi_{\mathrm{I}} = \frac{igA}{\omega}\frac{\cosh k_0(h+z)}{\cosh k_0 h} \mathrm{e}^{-ik_0(x\cos\beta + y\sin\beta)} \tag{43}$$

where the origin is fixed on the free surface and the z axis is pointing upwards. Equation (43) can be expanded to non-axisymmetric prolate spheroidal coordinates according to (see Wu and Eatock Taylor 1987; Chatjigeorgiou and Miloh 2014a)

$$\phi_{\mathrm{I}} = \frac{igA}{\omega}\sum_{n=0}^{\infty}\sum_{m=0}^{n} (B_n^m \cos m\psi + i\tilde{B}_n^m \sin m\psi) \times P_n^m(\mu) P_n^m(\zeta), \tag{44}$$

where

$$B_n^m = \frac{\mathrm{e}^{k_0(h-f)} + (-1)^m e^{-k_0(h-f)}}{2\cosh k_0 h}(-1)^{n+m}\frac{\varepsilon_m}{2} \times i^{n+m}\frac{(n-m)!}{(n+m)!}(2n+1)N_m(\beta) \times \left(\frac{\pi}{2k_0\cos\beta}\right)^{1/2} J_{n+1/2}(k_0\cos\beta), \tag{45}$$

$$\tilde{B}_n^m = \frac{\mathrm{e}^{k_0(h-f)} - (-1)^m e^{-k_0(h-f)}}{2\cosh k_0 h}(-1)^{n+m+1}\frac{\varepsilon_m}{2} \times i^{n+m}\frac{(n-m)!}{(n+m)!}(2n+1)\tilde{N}_m(\beta) \times \left(\frac{\pi}{2k_0\cos\beta}\right)^{1/2} J_{n+1/2}(k_0\cos\beta). \tag{46}$$

Using the auxiliary multipole expansions of the Green's function Eq. (16), the diffraction potential is written as

$$\phi_{\mathrm{D}} = \frac{igA}{\omega}\sum_{n=0}^{\infty}\sum_{m=0}^{n} F_n^m \left\{ P_n^m(\mu) Q_n^m(\zeta)\mathrm{e}^{im\psi} + \sum_{s=0}^{\infty}\sum_{t=0}^{s} (C_{ns}^{mt}\cos t\psi + i\tilde{C}_{ns}^{mt}\sin t\psi)\, P_s^t(\mu) P_s^t(\zeta) \right\}, \tag{47}$$

where F_n^m denote herein the unknown expansion coefficients associated with the diffraction problem. These are obtained by invoking the Neumann body boundary condition, which in spheroidal coordinates reads

$$\frac{\partial\phi_{\mathrm{D}}}{\partial\zeta} = -\frac{\partial\phi_{\mathrm{I}}}{\partial\zeta}, \quad \zeta = \zeta_0 = \cosh u_0. \tag{48}$$

Substituting Eqs. (44) and (47) into Eq. (48) and making use of the orthogonality relations of both the trigonometric and the associated Legendre functions of the first kind (Abramowitz and Stegun 1970), leads to the following complex linear systems in terms of the unknown expansion coefficients F_n^m:

$$F_l^r + \alpha_l^r \sum_{n=0}^{\infty}\sum_{m=0}^{n} F_n^m C_{nl}^{mr} = -B_l^r \alpha_l^r, \tag{49}$$

$$\hat{F}_l^r + \alpha_l^r \sum_{n=0}^{\infty}\sum_{m=0}^{n} \tilde{F}_n^m \tilde{C}_{nl}^{mr} = -\tilde{B}_l^r \alpha_l^r. \tag{50}$$

The above relations are associated respectively with the cosine and the sine terms. The employment of the appropriate coefficients depends on the particular loading component that is considered, as demonstrated below.

It is evident that for the numerical computations the above Eqs. (49) and (50) must be truncated to account for a specific number of modes, whilst this number depends on the required accuracy. For most of the cases considered in the present and analyzed in the sequel, the employment of $N = 8$ modes resulted in convergence up to the fourth significant digit for the complete range of frequencies (up to $Ka = 5$). In fact, in the low frequency range the convergence is nearly immediate. It should be also mentioned that the water depth does not actually affect the number of harmonics (truncation) which are required for achieving convergence.

The exciting forces and moments are obtained by integrating the linear hydrodynamic pressure over the wetted surface of the body. Thus,

$$\mathbf{F} = -i\omega\rho\int_{S_0} (\phi_{\mathrm{I}} + \phi_{\mathrm{D}})\mathbf{n}\mathrm{d}S, \tag{51}$$

$$\mathbf{M} = -i\omega\rho\int_{S_0} (\phi_{\mathrm{I}} + \phi_{\mathrm{D}})(\mathbf{r}\times\mathbf{n})\mathrm{d}S, \tag{52}$$

where the unit vector **n** is given by Eq. (35). The employment of Eqs. (51)–(52) result in closed form relations for all hydrodynamic loading components. The final forms of the surge, sway, heave, pitch and yaw loadings can be found in reference (Chatjigeorgiou and Miloh 2014b).

6 Numerical results

6.1 Added mass and damping coefficients

Our method has been exhaustively validated against exiting data in the open literature. For the diffraction and radiation problems in finite (constant) water depths, the available calculations found concerned only spheres. For spheroids, no shallow water associated data were found. The existing numerical predictions which could be used as a benchmark to validate our method concerned therefore only the case of deep water.

A spheroid can effectively simulate a sphere by assuming $b \to a$. This is the case examined in Figs. 1 and 2 that concern a sphere immersed at $f = 1.25a$ in water depth $h = 5a$ (a herein denotes the radius of the sphere). The test case was taken from the work of Das and Mandal (2008) who studied the radiation problem for a sphere immersed below an ice cover. The case of a free upper surface was simulated by letting the stiffness of the ice cover D equal to zero. Das and Mandal (2008) reported calculations up to $Ka = 2$ and we have extended the computations range up to $Ka = 5$. The depicted data for the heave and sway hydrodynamic coefficients are normalized by the water displaced by the sphere

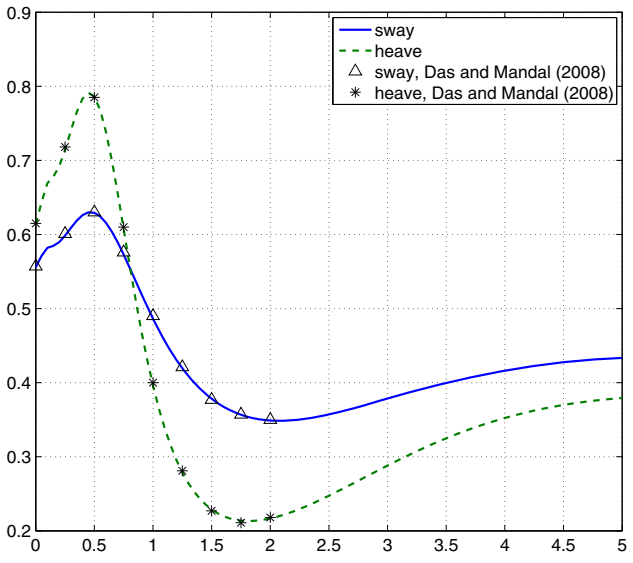

Fig. 1 Added mass coefficients for sway and heave μ_{22} and μ_{33} (against Ka), for a sphere immersed at $f = 1.25a$ below the free surface and finite water depth $h = 5a$

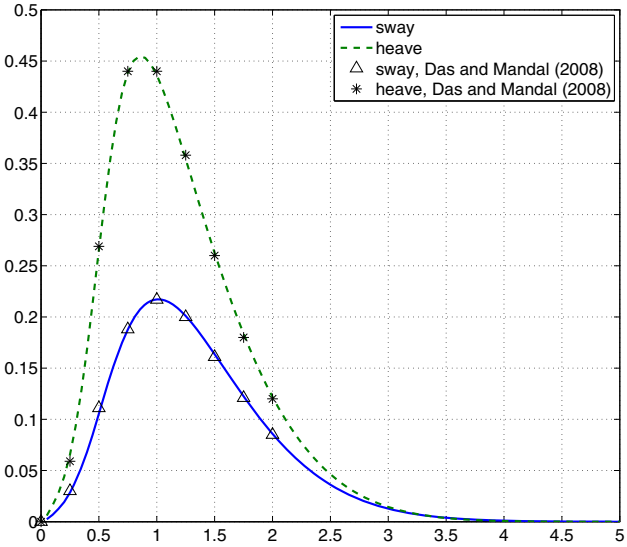

Fig. 2 Hydrodynamic damping coefficients for sway and heave λ_{22} and λ_{33} (against Ka) for a sphere immersed at $f = 1.25a$ below the free surface and finite water depth $h = 5a$

$4/3\pi\rho a^3$. It is immediately evident that the comparisons with Das and Mandal (2008) are very favorable which apparently demonstrate the efficacy of our method and the accuracy of our computations.

Comparative results for a spheroid assuming deep water are simulated in our method by letting $h = 200b$. Tables 1 and 2 show respectively computations of the added mass and the damping coefficients for the translational modes compared against the results reported by Wu and Eatock Taylor (1989), which were explicitly obtained for deep water. Similar results (not shown here) were also obtained for the corresponding rotational modes and show again favorable agreement with those reported in Wu and Eatock Taylor (1989). For most of the investigated components and for the majority of the normalized frequencies Ka, a coincidence up to the 4th significant digit is observed. The added masses are given normalized by $4/3\pi\rho ab^2$ and $4/15\pi\rho a^3b^2$ for the translational and rotational modes respectively. To achieve the favorable coincidence shown in Table 2 for the damping coefficients we had to normalize our results by $4/3\pi\rho ab^2\sqrt{Kbg/a}$ and $4/15\pi\rho a^3b^2\sqrt{Kbg/a}$ and we believe that this was also the normalization factor employed by Wu and Eatock Taylor (1989), although not specifically mentioned in their study.

The effect of variable water depth on the hydrodynamic coefficients is further examined with the aid of Figs. 3, 4, 5, 6, 7, 8, 9, 10, 11 and 12 for spheroid slenderness of $a/b = 6$ and submergence at $f = 2b$. Results are provided for all non-vanishing diagonal (five) terms of the added masses and damping coefficients for four different water depths, the first of which $h = 200b$ literally rep-

Table 1 Added mass coefficients for surge, sway and heave for a spheroid $a/b = 6$ immersed at $f = 2b$ in deep water $h = 200b$

Ka	μ_{11}		μ_{22}		μ_{33}	
	Present	Wu and Eatock Taylor (1989)	Present	Wu and Eatock Taylor (1989)	Present	Wu and Eatock Taylor (1989)
0.0	0.0532	0.0532	0.9861	0.9860	1.0155	1.0154
0.1	0.0544	0.0544	0.9928	0.9926	1.0266	1.0264
0.2	0.0558	0.0558	1.0001	1.0003	1.0396	1.0397
0.3	0.0575	0.0575	1.0090	1.0091	1.0550	1.0551
0.4	0.0593	0.0593	1.0189	1.0188	1.0722	1.0720
0.5	0.0611	0.0611	1.0291	1.0289	1.0899	1.0896
0.6	0.0628	0.0628	1.0393	1.0392	1.1072	1.1071
0.7	0.0644	0.0644	1.0491	1.0492	1.1234	1.1235
0.8	0.0657	0.0658	1.0584	1.0589	1.1378	1.1387
0.9	0.0666	0.0666	1.0668	1.0671	1.1493	1.1496
1.0	0.0671	0.0671	1.0740	1.0743	1.1573	1.1576
1.5	0.0618	0.0618	1.0840	1.0839	1.1302	1.1301
2.0	0.0457	0.0457	1.0465	1.0462	1.0124	1.0121
2.5	0.0283	0.0283	0.9793	0.9793	0.8821	0.8821
3.0	0.0185	0.0185	0.9075	0.9077	0.7905	0.7906
3.5	0.0170	0.0170	0.8467	0.8469	0.7411	0.7414
4.0	0.0198	0.0197	0.8015	0.8009	0.7175	0.7169
4.5	0.0231	0.0231	0.7712	0.7712	0.7050	0.7050
5.0	0.0254	0.0254	0.7522	0.7521	0.6964	0.6963

Table 2 Damping coefficients for surge, sway and heave for a spheroid $a/b = 6$ immersed at $f = 2b$ in deep water $h = 200b$

Ka	λ_{11}		λ_{22}		λ_{33}	
	Present	Wu and Eatock Taylor (1989)	Present	Wu and Eatock Taylor (1989)	Present	Wu and Eatock Taylor (1989)
0.0	0.0000	0.0000	0.0000	0.0000	0.0000	0.0000
0.1	0.0000	0.0000	0.0000	0.0000	0.0001	0.0001
0.2	0.0001	0.0001	0.0005	0.0005	0.0010	0.0010
0.3	0.0005	0.0005	0.0018	0.0018	0.0038	0.0038
0.4	0.0013	0.0013	0.0046	0.0047	0.0097	0.0098
0.5	0.0026	0.0026	0.0095	0.0096	0.0201	0.0202
0.6	0.0045	0.0045	0.0170	0.0171	0.0358	0.0360
0.7	0.0072	0.0072	0.0274	0.0275	0.0578	0.0582
0.8	0.0106	0.0106	0.0410	0.0412	0.0865	0.0871
0.9	0.0147	0.0148	0.0579	0.0583	0.1220	0.1228
1.0	0.0194	0.0196	0.0783	0.0789	0.1641	0.1652
1.5	0.0495	0.0498	0.2236	0.2251	0.4369	0.4397
2.0	0.0740	0.0745	0.3981	0.4006	0.6789	0.6831
2.5	0.0765	0.0770	0.5398	0.5432	0.7781	0.7830
3.0	0.0597	0.0600	0.6188	0.6229	0.7586	0.7636
3.5	0.0384	0.0387	0.6389	0.6433	0.6911	0.6958
4.0	0.0233	0.0234	0.6176	0.6212	0.6222	0.6257
4.5	0.0158	0.0159	0.5732	0.5773	0.5647	0.5687
5.0	0.0128	0.0128	0.5181	0.5217	0.5122	0.5158

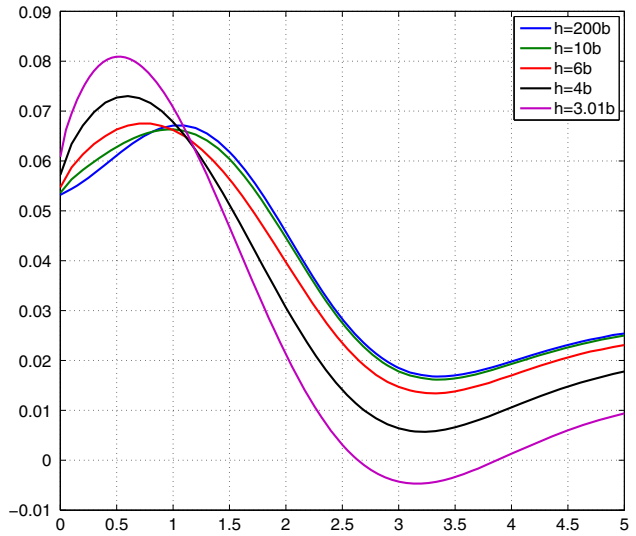

Fig. 3 Normalized surge added mass coefficients μ_{11} (against Ka), of a prolate spheroid $a/b = 6$, immersed at $f = 2b$ bellow the free surface for various (constant) water depths

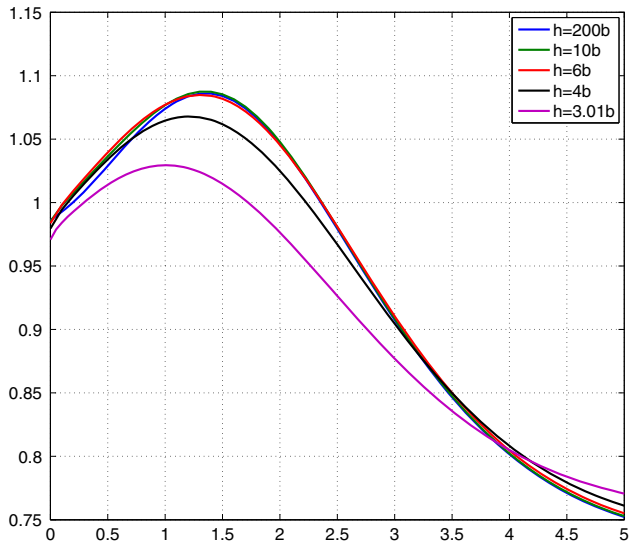

Fig. 4 Normalized sway added mass coefficients μ_{22} (against Ka), of a prolate spheroid $a/b = 6$, immersed at $f = 2b$ bellow the free surface for various (constant) water depths

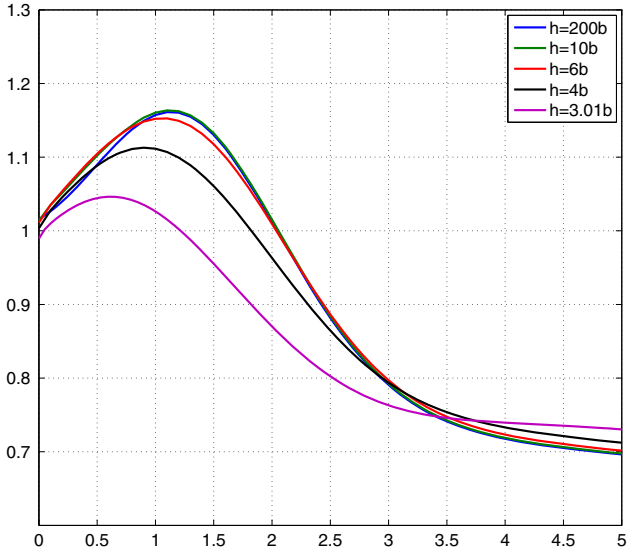

Fig. 5 Normalized heave added mass coefficients μ_{33} (against Ka), of a prolate spheroid $a/b = 6$, immersed at $f = 2b$ bellow the free surface for various (constant) water depths

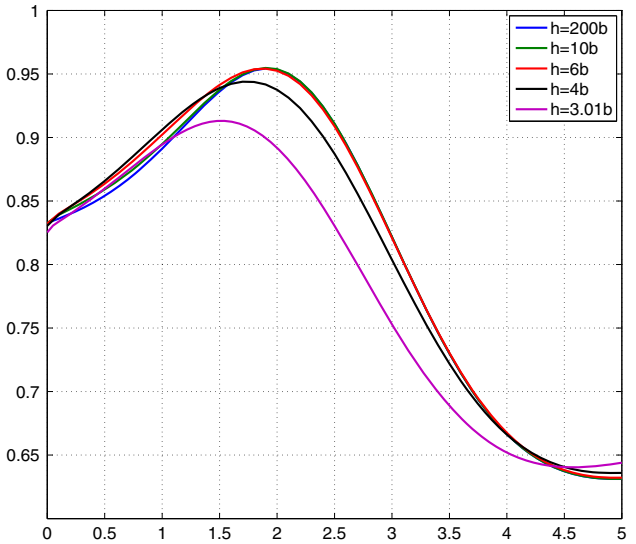

Fig. 6 Normalized pitch added mass coefficients μ_{55} (against Ka), of a prolate spheroid $a/b = 6$, immersed at $f = 2b$ bellow the free surface for various (constant) water depths

resents the infinite water depth case. Finite and shallow water depth cases are those corresponding to $h = 10b$, $6b$, $4b$ and $3.01b$, where the last case corresponds to a bottom touching configuration. It is immediately evident that decreasing water depths result in significant differentiations of added masses at the low frequency regions. The differences tend to vanish at the high frequency regions with the only exception that of the surge added mass μ_{11} (see Fig. 3). Note also the negative values around $Ka = 3$ for the bottom seated case which arise due to small clearance from the sea floor. As regards the hydrodynamic damping coefficients, it is remarked that only the very shallow water depth cases $h = 4b$ and $h = 3.01b$ are completely detached from the usual trend, factually provided by the deep water case. These cases however are the most interesting since they indicate that shallow water significantly increases hydrodynamic damping.

6.2 Exciting diffraction forces and moments

The hydrodynamic loadings due to oblique wave diffraction exerted on the spheroid ($a/b = 6$, $f = 2b$) for variable water

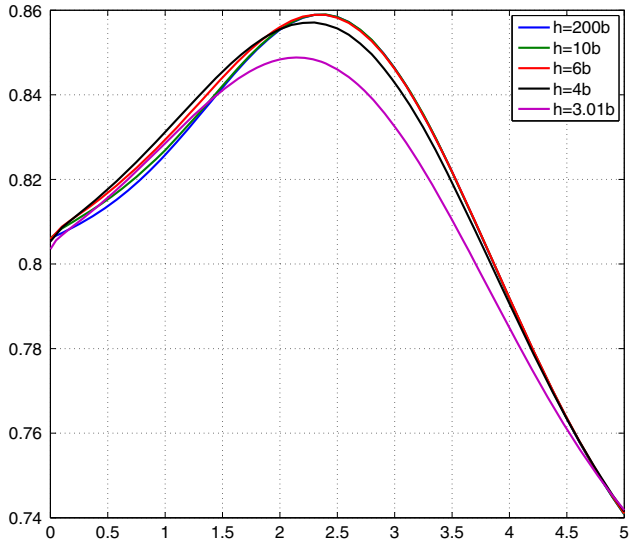

Fig. 7 Normalized yaw added mass coefficients μ_{66} (against Ka), of a prolate spheroid $a/b = 6$, immersed at $f = 2b$ bellow the free surface for various (constant) water depths

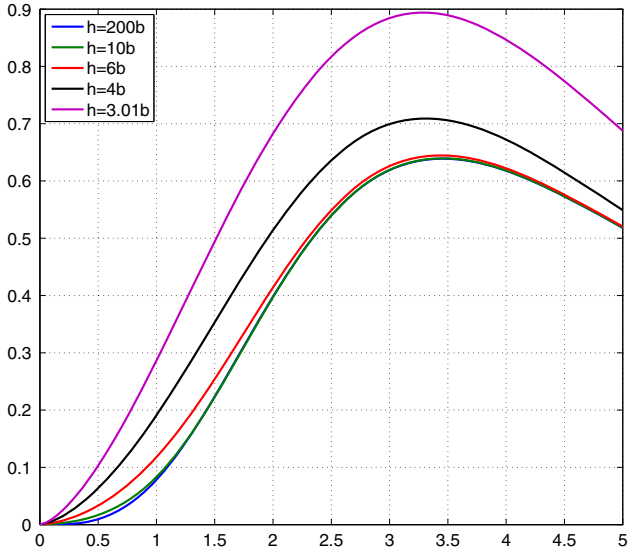

Fig. 9 Normalized sway hydrodynamic damping coefficients λ_{22} (against Ka), of a prolate spheroid $a/b = 6$, immersed at $f = 2b$ bellow the free surface for various (constant) water depths

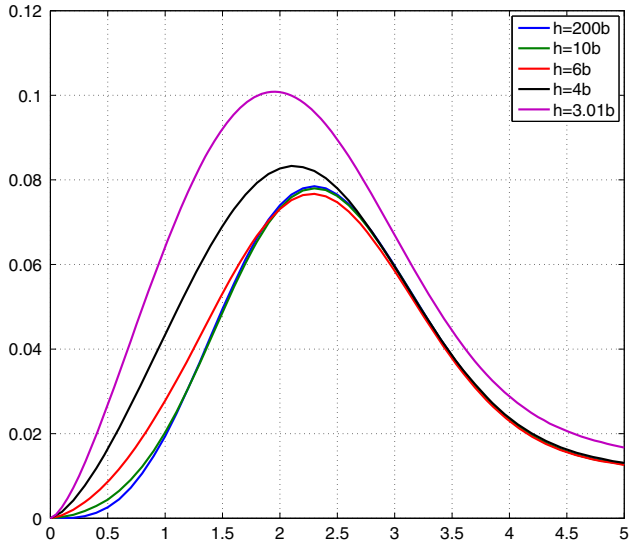

Fig. 8 Normalized surge hydrodynamic damping coefficients λ_{11} (against Ka), of a prolate spheroid $a/b = 6$, immersed at $f = 2b$ bellow the free surface for various (constant) water depths

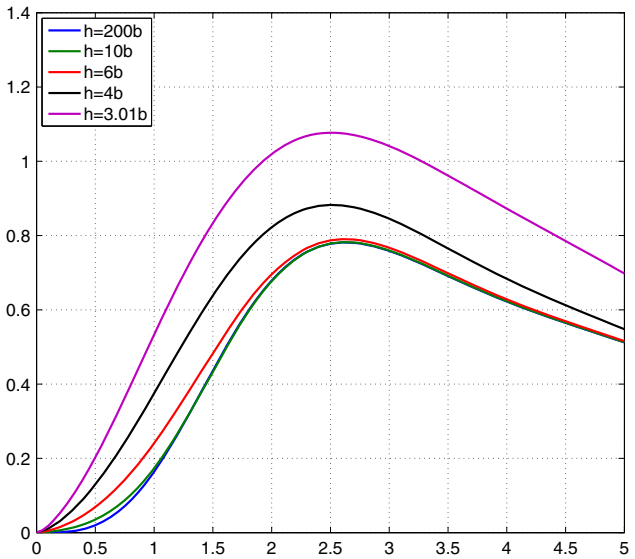

Fig. 10 Normalized heave hydrodynamic damping coefficients λ_{33} (against Ka), of a prolate spheroid $a/b = 6$, immersed at $f = 2b$ bellow the free surface for various (constant) water depths

depths, are examined with the aid of Figs. 13, 14, 15, 16, 17, 18, 19, 20, 21, 22, 23, 24, 25, 26, 27, 28, 29, 30, 31 and 32. The results have been normalized by $4/3\pi ab^2\rho gAK\exp(-Kf)$ for the forces and by $4/3\pi ab^3\rho gAK\exp(-Kf)$ for the moments. Here, the real and the imaginary parts are provided separately. Three angles of heading were considered, i.e. $\beta = 0°$, (Figs. 13, 14, 15, 16, 17, 18), $\beta = 45°$, (Figs. 19, 20, 21, 22, 23, 24, 25, 26, 27, 28) and $\beta = 90°$, (Figs. 29, 30, 31, 32). The infinite water depth case was simulated assuming, again $h = 200b$, whereas the results marked as $h =$ infinity coincide explicitly that of Wu and Eatock Taylor (1989). Again our predictions show extremely favorable coincidence with the existing data reported in Wu and Eatock Taylor (1987) and Wu and Eatock Taylor (1989). The main conclusions that could be drawn from inspecting the trends depicted in Figs. 13, 14, 15, 16, 17, 18, 19, 20, 21, 22, 23, 24, 25, 26, 27, 28, 29, 30, 31 and 32, are summarized succinctly in the following: (i) Shallow water effects diminish for high wave

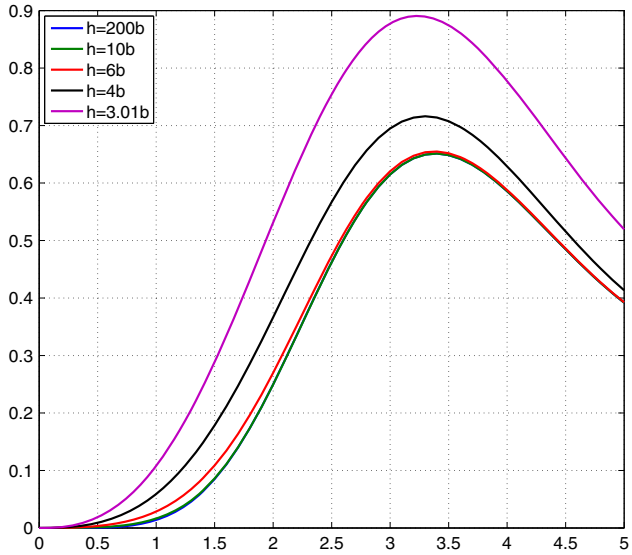

Fig. 11 Normalized pitch hydrodynamic damping coefficients λ_{55} (against Ka), of a prolate spheroid $a/b = 6$, immersed at $f = 2b$ bellow the free surface for various (constant) water depths

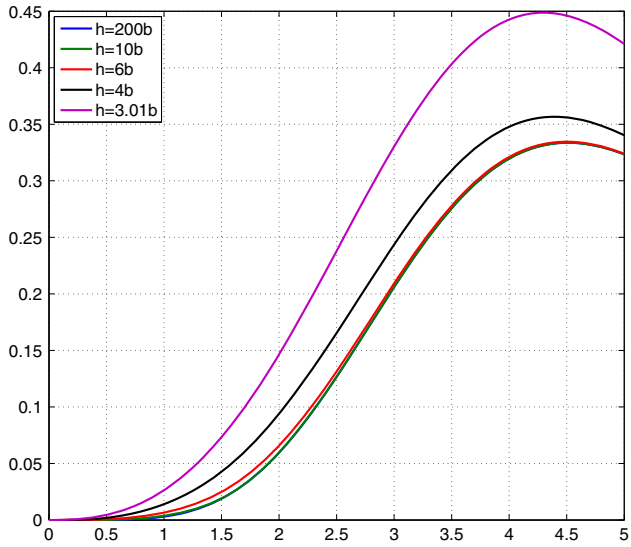

Fig. 12 Normalized yaw hydrodynamic damping coefficients λ_{66} (against Ka), of a prolate spheroid $a/b = 6$, immersed at $f = 2b$ bellow the free surface for various (constant) water depths

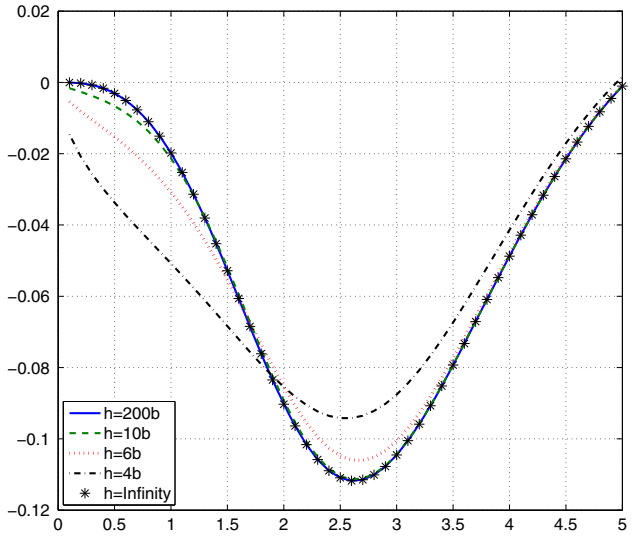

Fig. 13 Real part of the normalized surge exciting forces $\mathrm{Re}(f_x)$ (against Ka), acting on a prolate spheroid $a/b = 6$, immersed at $f = 2b$, below the free surface for various (constant) water depths and wave heading angle $\beta = 0°$ with respect to the spheroid's semi-major axis

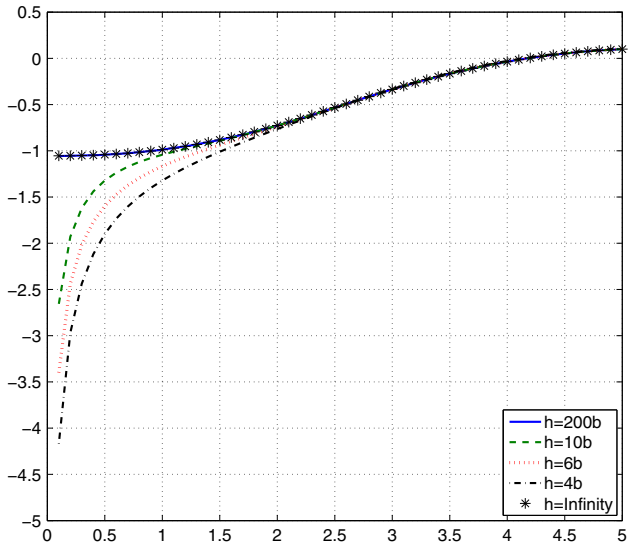

Fig. 14 Imaginary part of the normalized surge exciting forces $\mathrm{Im}(f_x)$ (against Ka), acting on a prolate spheroid $a/b = 6$, immersed at $f = 2b$, below the free surface for various (constant) water depths and wave heading angle $\beta = 0°$ with respect to the spheroid's semi-major axis

frequencies; (ii) the magnitudes of the heave forces decrease for deceasing water depths; (iii) the opposite condition is observed for the surge and sway forces (irrespectively of the heading angle), which demonstrate large amplifications for $Ka \to 0$; (iv) the pitch moments exhibit a small increase for small frequencies (compared to $h \to \infty$) which is followed by significant reductions for decreasing water depths; (v) the magnitudes of the pitch moments tend to some non- vanishing values as $Ka \to 0$ in shallow water; (vi) yaw moments (here examined only for $\beta = 45°$) are also found to exhibit large amplifications for decreasing water depths in the small wave frequency range, attaining again some finite values for wave frequencies approaching zero.

7 Conclusions

The present concluding study follows a series of papers (Chatjigeorgiou and Miloh 2013, 2014a, b) which analytically solve relevant hydrodynamic linearized free-surface

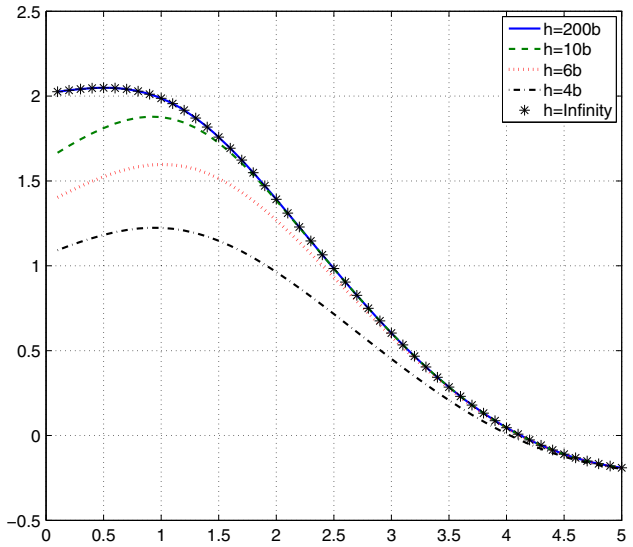

Fig. 15 Real part of the normalized heave exciting forces $\mathrm{Re}(f_z)$ (against Ka), acting on a prolate spheroid $a/b = 6$, immersed at $f = 2b$, below the free surface for various (constant) water depths and wave heading angle $\beta = 0°$ with respect to the spheroid's semi-major axis

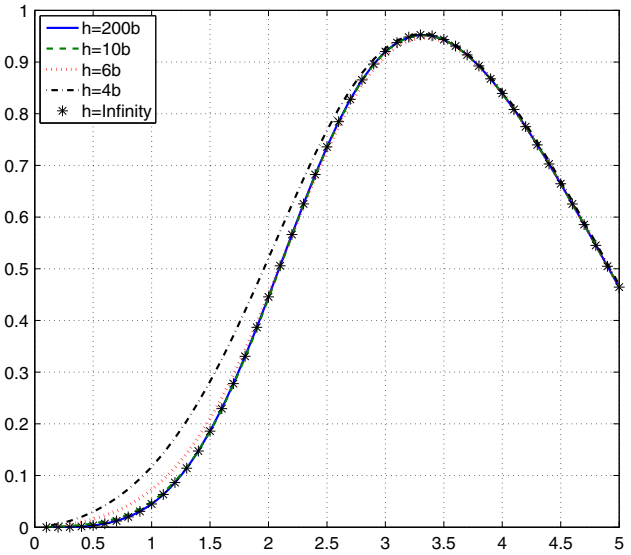

Fig. 17 Real part of the normalized pitch exciting moment $\mathrm{Re}(m_y)$ (against Ka), acting on a prolate spheroid $a/b = 6$, immersed at $f = 2b$, below the free surface for various (constant) water depths and wave heading angle $\beta = 0°$ with respect to the spheroid's semi-major axis

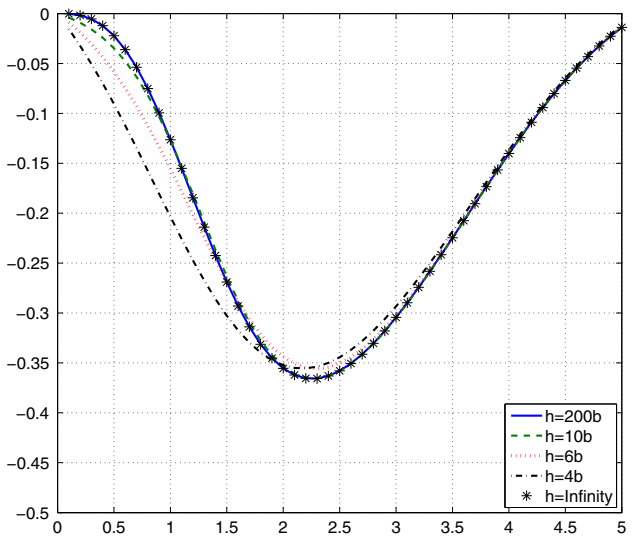

Fig. 16 Imaginary part of the normalized heave exciting forces $\mathrm{Im}(f_z)$ (against Ka), acting on a prolate spheroid $a/b = 6$, immersed at $f = 2b$, below the free surface for various (constant) water depths and wave heading angle $\beta = 0°$ with respect to the spheroid's semi-major axis

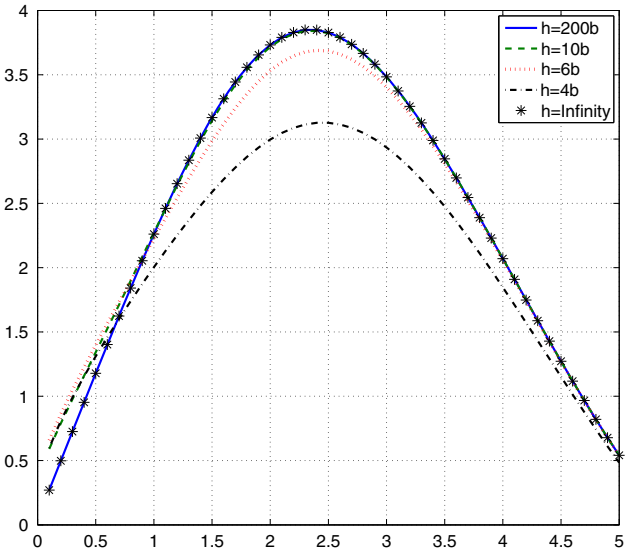

Fig. 18 Imaginary part of the normalized pitch exciting moment $\mathrm{Im}(m_y)$ (against Ka), acting on a prolate spheroid $a/b = 6$, immersed at $f = 2b$, below the free surface for various (constant) water depths and wave heading angle $\beta = 0°$ with respect to the spheroid's semi-major axis

problems of an elongated fully submerged axisymmetric shape (simulated by a prolate spheroid) positioned in water of arbitrary depth. The wave diffraction (scattering) problem of a fixed spheroid in deep water in the presence of a monochromatic wave train of any angle of incidence was first discussed in Chatjigeorgiou and Miloh (2013). The case of a forward-speed combined with wave diffraction in deep water was then elaborated in Chatjigeorgiou and Miloh (2014a), where the solution for the wave-resistance problem is given as a limiting case. The effect of water of finite (shallow) depth on the wave resistance and diffraction (zero wave heading), was finally analyzed in Chatjigeorgiou and Miloh (2014b). In order to expound the full (six degrees of freedom) motion problem of a spheroid in confined water, we provide herein the solution

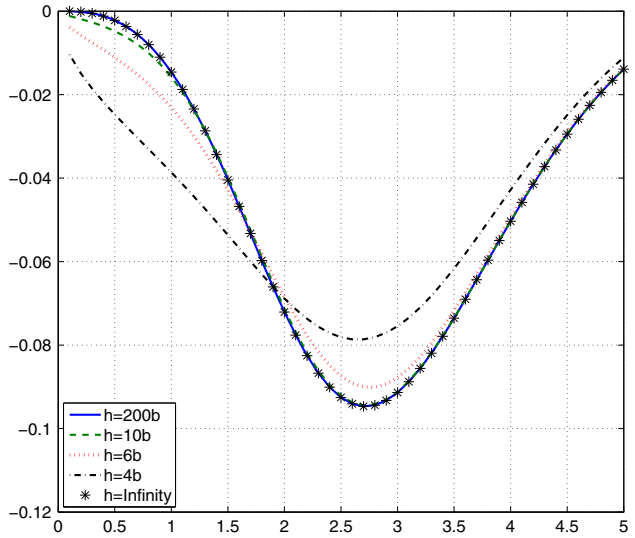

Fig. 19 Real part of the normalized surge exciting forces $\mathrm{Re}(f_x)$ (against Ka), acting on a prolate spheroid $a/b = 6$, immersed at $f = 2b$, below the free surface for various (constant) water depths and wave heading angle $\beta = 45°$ with respect to the spheroid's semi-major axis

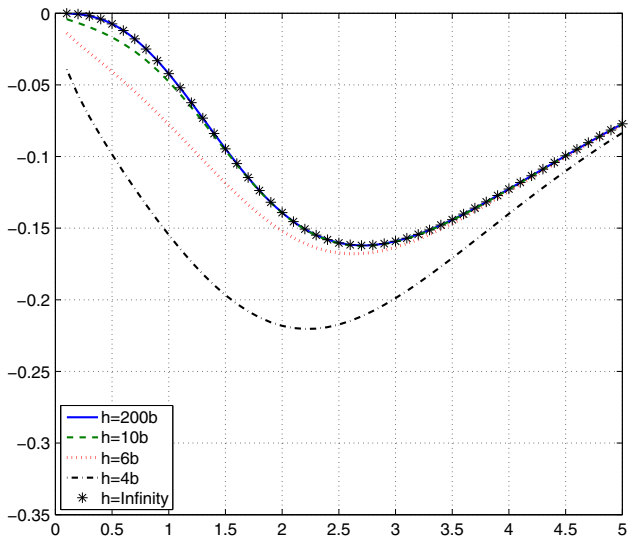

Fig. 21 Real part of the normalized sway exciting forces $\mathrm{Re}(f_y)$ (against Ka), acting on a prolate spheroid $a/b = 6$, immersed at $f = 2b$, below the free surface for various (constant) water depths and wave heading angle $\beta = 45°$ with respect to the spheroid's semi-major axis

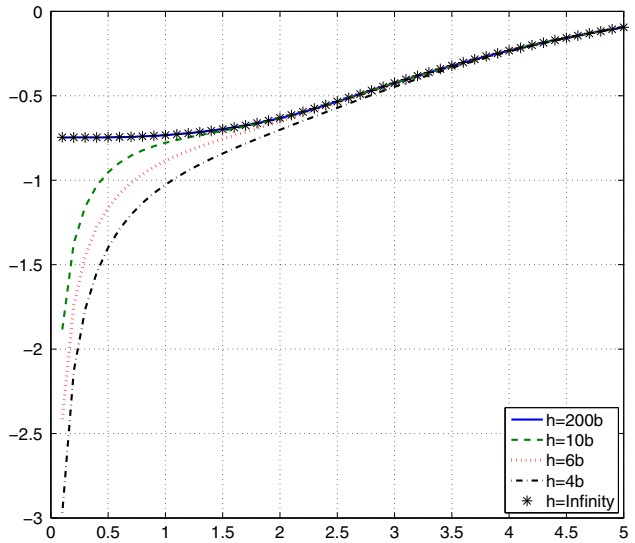

Fig. 20 Imaginary part of the normalized surge exciting forces $\mathrm{Im}(f_x)$ (against Ka), acting on a prolate spheroid $a/b = 6$, immersed at $f = 2b$, below the free surface for various (constant) water depths and wave heading angle $\beta = 45°$ with respect to the spheroid's semi-major axis

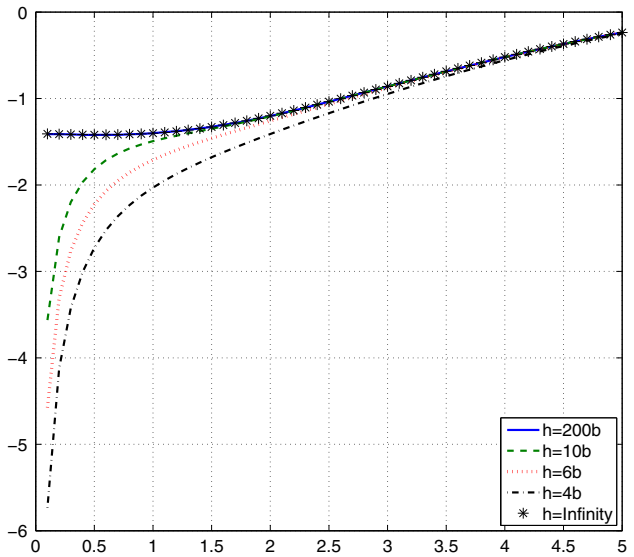

Fig. 22 Imaginary part of the normalized sway exciting forces $\mathrm{Im}(f_y)$ (against Ka), acting on a prolate spheroid $a/b = 6$, immersed at $f = 2b$, below the free surface for various (constant) water depths and wave heading angle $\beta = 45°$ with respect to the spheroid's semi-major axis

for the various added-mass and damping depth-dependent coefficients as well as explicit expressions for the wave diffraction (due to a monochromatic wave-train) exerted on the submerged spheroid for various wave headings and water depths. Extreme cases, such as small submergence under a free-surface or small bottom clearance are also given, including extensive numerical validations against known solutions for spherical geometries.

The general methodology employed, is based on using Havelock's spheroid theorem and on expanding the relevant Green's function in terms of external spheroidal harmonics which can be expressed as multipole distributions on the axis between the two foci. It has been also demonstrated that the proposed formulation can be facilely numerically implemented. Furthermore the present numerical scheme (based on extending the analysis as far as possible) was

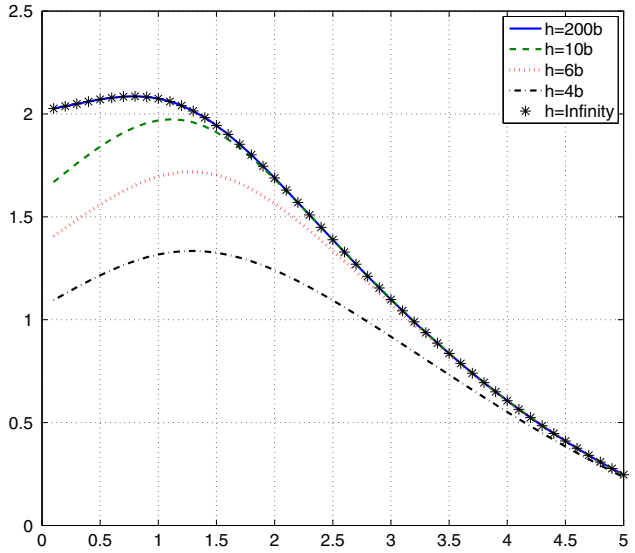

Fig. 23 Real part of the normalized heave exciting forces $\mathrm{Re}(f_z)$ (against Ka), acting on a prolate spheroid $a/b = 6$, immersed at $f = 2b$, below the free surface for various (constant) water depths and wave heading angle $\beta = 45°$ with respect to the spheroid's semi-major axis

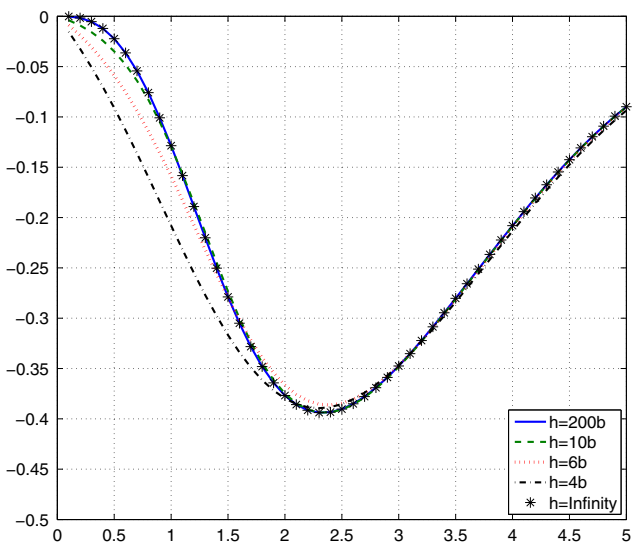

Fig. 24 Imaginary part of the normalized heave exciting forces $\mathrm{Im}(f_z)$ (against Ka), acting on a prolate spheroid $a/b = 6$, immersed at $f = 2b$, below the free surface for various (constant) water depths and wave heading angle $\beta = 45°$ with respect to the spheroid's semi-major axis

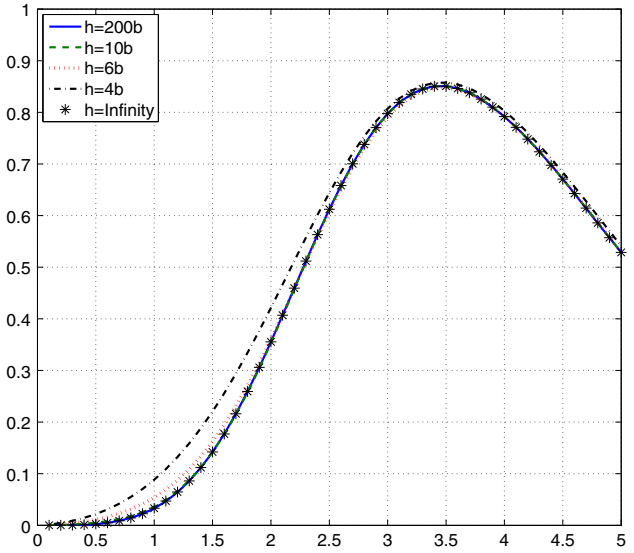

Fig. 25 Real part of the normalized pitch exciting moment $\mathrm{Re}(m_y)$ (against Ka), acting on a prolate spheroid $a/b = 6$, immersed at $f = 2b$, below the free surface for various (constant) water depths and wave heading angle $\beta = 45°$ with respect to the spheroid's semi-major axis

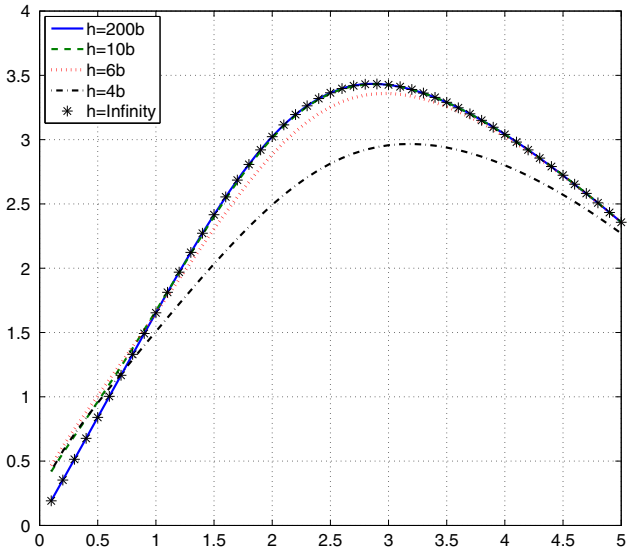

Fig. 26 Imaginary part of the normalized pitch exciting moment $\mathrm{Im}(m_y)$ (against Ka), acting on a prolate spheroid $a/b = 6$, immersed at $f = 2b$, below the free surface for various (constant) water depths and wave heading angle $\beta = 45°$ with respect to the spheroid's semi-major axis

found to be robust and efficient compared to full numerical codes based on solving a Fredholm integral (of the second kind) for the unknown source distribution over the spheroidal body.

Finally, it is remarked that the current semi-analytic approach and the vast number of numerical simulations (graphically plotted) thus performed, can be applied for factual hydrodynamic studies, such as wave-diffraction, radiation, wave resistance, maneuvering and stability of practical vessels which can be approximated by an "equivalent" prolate spheroid. By admitting this "equivalence" dogma, one can replace any axisymmetric body by a "corresponding" prolate spheroid having the same volume and slenderness-ratio. By doing so, one can readily establish all the impor-

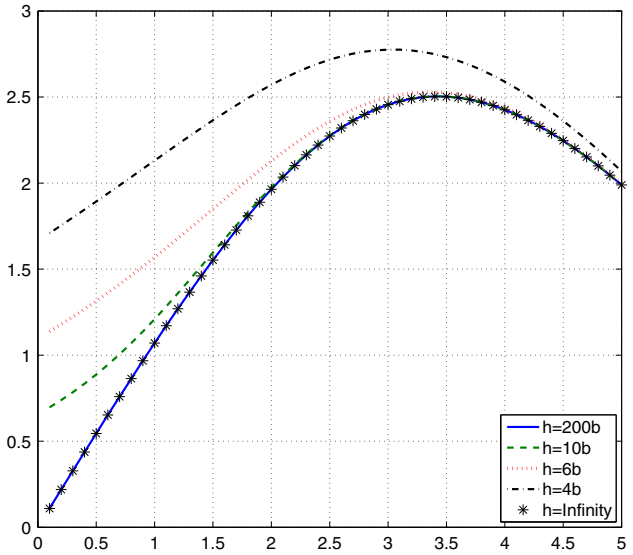

Fig. 27 Real part of the normalized yaw exciting moment $\mathrm{Re}(m_z)$ (against Ka), acting on a prolate spheroid $a/b = 6$, immersed at $f = 2b$, below the free surface for various (constant) water depths and wave heading angle $\beta = 45°$ with respect to the spheroid's semi-major axis

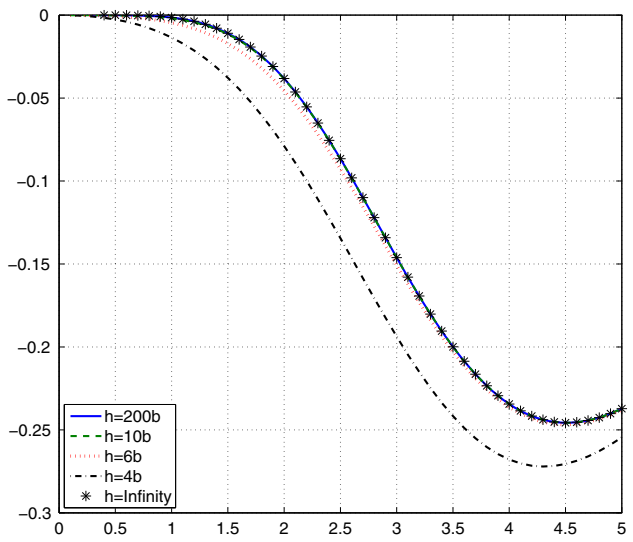

Fig. 28 Imaginary part of the normalized yaw exciting moment $\mathrm{Im}(m_z)$ (against Ka), acting on a prolate spheroid $a/b = 6$, immersed at $f = 2b$, below the free surface for various (constant) water depths and wave heading angle $\beta = 45°$ with respect to the spheroid's semi-major axis

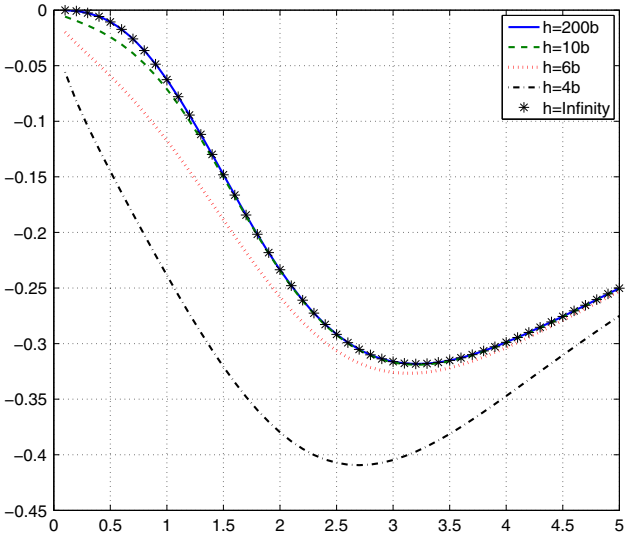

Fig. 29 Real part of the normalized sway exciting forces $\mathrm{Re}(f_y)$ (against Ka), acting on a prolate spheroid $a/b = 6$, immersed at $f = 2b$, below the free surface for various (constant) water depths and wave heading angle $\beta = 90°$ with respect to the spheroid's semi-major axis

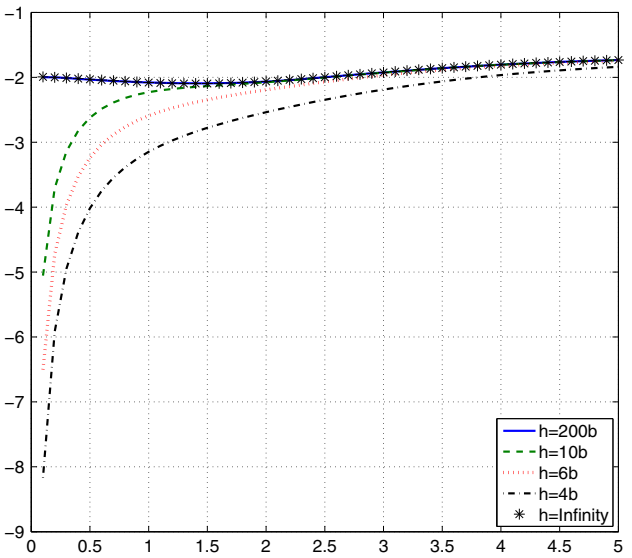

Fig. 30 Imaginary part of the normalized sway exciting forces $\mathrm{Im}(f_y)$ (against Ka), acting on a prolate spheroid $a/b = 6$, immersed at $f = 2b$, below the free surface for various (constant) water depths and wave heading angle $\beta = 90°$ with respect to the spheroid's semi-major axis

tant hydrodynamical parameters for the practitioner, such as wave-resistance, diffraction forces and moments for arbitrary wave heading, added-mass and damping coefficients, etc. All relevant parameters are obtained for the case of a spheroid whose major axis is parallel to the undisturbed free-surface (or to the even rigid bottom) but otherwise are valid for arbitrary slenderness-ratios (including spheres) depth of submergence, water depth and Froude number, wave encounter frequency and angle of incidence of the ambient wave-train.

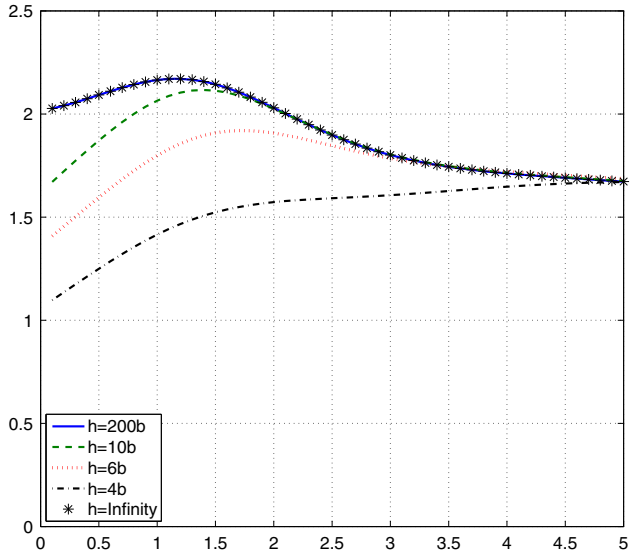

Fig. 31 Real part of the normalized heave exciting forces $\mathrm{Re}(f_z)$ (against Ka), acting on a prolate spheroid $a/b = 6$, immersed at $f = 2b$, below the free surface for various (constant) water depths and wave heading angle $\beta = 90°$ with respect to the spheroid's semi-major axis

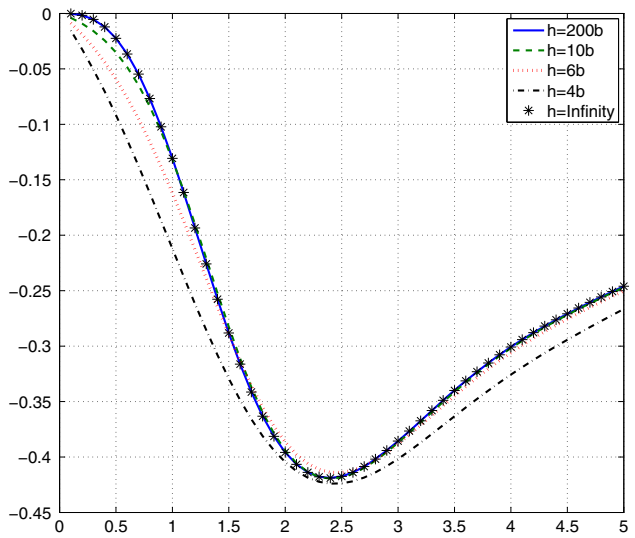

Fig. 32 Imaginary part of the normalized heave exciting forces $\mathrm{Im}(f_z)$ (against Ka), acting on a prolate spheroid $a/b = 6$, immersed at $f = 2b$, below the free surface for various (constant) water depths and wave heading angle $\beta = 90°$ with respect to the spheroid's semi-major axis

References

Abramowitz M, Stegun IA (1970) Handbook of mathematical functions. Dover Publications Inc., New York

Bialecki B, Keast P (1999) A sinc quadrature subroutine for Cauchy principal value integrals. J Comput Appl Math 112:3–20

Chatjigeorgiou IK (2012) Hydrodynamic exciting forces on a submerged oblate spheroid in regular waves. Comp Fluids 57:151–162. doi:10.1016/j.compfluid.2011.12.013

Chatjigeorgiou IK (2013) The analytic solution for hydrodynamic diffraction by submerged prolate spheroids in infinite water depth. J Eng Math 81:47–65. doi:10.1007/s10665-012-9581-x

Chatjigeorgiou IK, Miloh T (2013) Wave scattering of spheroidal bodies bellow a free surface. J Ship Res 57:141–154. doi:10.5957/JOSR.57.2.120026

Chatjigeorgiou IK, Miloh T (2014a) Hydrodynamics of submerged prolate spheroids advancing under-waves: wave diffraction with forward speed. J Fluids Struct. doi:10.1016/j.jfluidstructs.2014.04.012

Chatjigeorgiou IK, Miloh T (2014b) Wave-making resistance and diffraction by spheroidal vessels in finite water. Q J Mech Appl Math (in press).

Das D, Mandal BN (2008) Water wave radiation by a sphere submerged in water with an ice-cover. Arch Appl Mech 78:649–661. doi:10.1007/s00419-007-0186-1

Farell C (1973) On the wave resistance of a submerged spheroid. J Ship Res 17:1–11

Gray EP (1979) Scattering of a surface wave by a submerged sphere. J Eng Math 12:15–41

Havelock TH (1954) The forces on a submerged body moving under waves. Trans Inst Naval Arch 96:77–88

Havelock TH (1955) Waves due to a floating sphere making periodic heaving oscillations. Proc R Soc Lond A 321:1–7

Hulme A (1982) The wave forces on a floating hemisphere undergoing forced periodic oscillations. J Fluid Mech 121:443–463

Linton CM (1991) Radiation and diffraction of water waves by a submerged sphere in finite depth. Ocean Eng 18:61–74

Miloh T (1974) The ultimate image singularities for external ellipsoidal harmonics. SIAM J Appl Math 26:334–344

Nicholson JW (1924) Oblate spheroidal harmonics and their applications. Phil Trans R Soc Lond A 224:49–93

Press WH, Flannery BP, Teukolsky SA, Vetterling WT (1986) Numerical recipes. Cambridge University Press, Cambridge

Rahman M (2001) Simulation of diffraction of ocean waves by a submerged sphere in finite depth. Appl Ocean Res 23:305–317

Srokosz MA (1979) The submerged sphere as an absorber of wave power. J Fluid Mech 95:717–741

Thorne RC (1953) Multipole expansions in the theory of surface waves. Proc Camb Phil Soc 49:709–716

Ursell F (1950) Surface waves on deep water in the presence of a submerged circular cylinder–I. Proc Camb Phil Soc 46:141–162

Wang A (1986) Motions of a spherical submarine in waves. Ocean Eng 13:249–271

Watson GN (1944) A treatise on the theory of Bessel functions, 2nd edn. Cambridge University Press, Cambridge

Wehausen JV, Laitone EV (1960) Surface waves. In: Flugge S, Truesdell C (eds) Handbuch der Physik, vol 9. Springer, Berlin, pp 446–778

Wu GX, Witz JA, Ma Q, Brown DT (1994) Analysis of wave induced drift forces acting on a submerged sphere in finite water depth. Appl Ocean Res 16:353–361

Wu GX, Eatock Taylor R (1987) The exciting force on a submerged spheroid in regular waves. J Fluid Mech 182:411–426

Wu GX, Eatock Taylor R (1989) On radiation and diffraction of surface waves by submerged spheroids. J Ship Res 33:84–92